Theory of $PbTiO_3$, $BaTiO_3$, and $SrTiO_3$ Surfaces

B. Meyer, J. Padilla, and David Vanderbilt
Department of Physics and Astronomy, Rutgers University, Piscataway, New Jersey 08855-0849
(March 1, 1999)

Abstract

First-principles total-energy calculations are carried out for (001) surfaces of the cubic perovskite $ATiO_3$ compounds $PbTiO_3$, $BaTiO_3$, and $SrTiO_3$. Both AO-terminated and TiO_2-terminated surfaces are considered, and fully-relaxed atomic configurations are determined. In general, $BaTiO_3$ and $SrTiO_3$ are found to have a rather similar behavior, while $PbTiO_3$ is different in many respects because of the partially covalent character of the Pb–O bonds. $PbTiO_3$ and $BaTiO_3$ are ferroelectrics, and the influence of the surface upon the ferroelectric distortions is studied for the case of a tetragonal ferroelectric distortion parallel to the surface. The surface relaxation energies are found to be substantial, i.e., many times larger than the bulk ferroelectric well depth. Nevertheless, the influence of the surface upon the ferroelectric order parameter is modest, and is qualitatively as well as quantitatively different for the two materials. Surface energies and electronic properties are also computed. It is found that for $BaTiO_3$ and $SrTiO_3$ surfaces, both AO-terminated and TiO_2-terminated surfaces can be thermodynamically stable, whereas for $PbTiO_3$ only the PbO surface termination is stable.

I. INTRODUCTION

The surfaces of insulating cubic perovskite materials such as $PbTiO_3$, $BaTiO_3$, and $SrTiO_3$ are of interest from several points of view. First, some of these materials (notably $SrTiO_3$) are very widely used as substrates for growth of other oxide materials (e.g., layered high-T_c superconductors and "colossal magnetoresistance" materials). Second, this class of materials is of enormous importance for actual and potential applications that make use of their unusual piezoelectric, ferroelectric, and dielectric properties (e.g., for piezoelectric transducers, non-volatile memories, and wireless communications applications, respectively). Many of these applications are increasingly oriented towards thin-film geometries, where surface properties are of growing importance. Third, the bulk materials display a variety of structural phase transitions; the ferroelectric (FE) structural phases are of special interest, but antiferroelectric (AFE) or antiferrodistortive (AFD) transitions can also take place.[1] It is then of considerable fundamental interest to consider how these structural distortions couple to the surface, e.g., whether the presence of the surface acts to enhance or suppress the structural distortion. The ferroelectric properties are well known to degrade in thin-film[2] and particulate[3] geometries, and it is very important to understand whether such behavior

is intrinsic to the presence of a surface, or whether it arises from extrinsic factors such as compositional non-uniformities or structural defects in the surface region. Finally, the cubic perovskites can serve as model systems for the study of transition-metal oxide surfaces more generally.[4]

In the last decade, there has been a surge of activity in the application of first-principles computational methods based on density-functional theory (DFT) to the study of the bulk properties, and especially the ferroelectric transitions, in bulk perovskite oxides. (For a recent review, see Ref. 5 or 6.) The importance of these methods was recently underlined by the award of the Nobel Prize in Chemistry to Walter Kohn, the primary originator of DFT. In the materials theory community, these methods have been widely used for two decades to predict properties of semiconductors and simple metals. However, recent advances in computational algorithms and computer power now allow these methods to be applied to more complex materials (e.g., perovskites) and more complex geometries (e.g., defects and surfaces). In particular, pioneering studies of $BaTiO_3$[7–9] and $SrTiO_3$[10–12] surfaces have recently appeared.

Experimental investigations of the surface structure of cubic perovskites have not been very extensive. Such studies are hindered by the difficulties of preparing clean and defect-free surfaces, and of overcoming charging effects associated with many experimental probes. Even for $SrTiO_3$, the best-studied of these surfaces, there is a disappointing level of agreement among experimental results[23–26] and between experiment and theory.[11] We are not aware of comparable studies of $BaTiO_3$ and $PbTiO_3$ surfaces.

The purpose of the present contribution is to present new theoretical work on the structural properties of the $PbTiO_3$ (001) surface, and to compare and contrast these results with the previous work of our group on $BaTiO_3$ and $SrTiO_3$ surfaces.[9,11] As regards bulk properties, lead-based compounds such as $PbTiO_3$ and $PbZrO_3$ are known to behave quite differently from alkaline-earth based perovskites such as $BaTiO_3$ and $SrTiO_3$. Previous theoretical work has shown that the FE distortion is typically larger and that Pb atoms participate much more strongly in (and sometimes even dominate) the FE distortion, compared with non-Pb perovskites.[13–17] Moreover, the Pb-based compounds are generally more susceptible to more complex AFD and AFE instabilities involving tilting of the oxygen octahedra,[16–19] and the ground-state structures often involve the formation of some quite short Pb–O bonds.[19–22] All of these effects point to a strong and active involvement of the Pb atoms in the bonding, most naturally interpreted in terms of the formation of partially covalent Pb–O bonds with the closest oxygen neighbors. Finally, a focus on Pb-based materials is motivated by the fact that these are the leading candidates for many practical piezoelectric and switching applications, especially in the form of solid solutions such as PZT ($PbZr_xTi_{1-x}O_3$), PMN ($PbMg_{1/3}Nb_{2/3}O_3$), and PZN ($PbZn_{1/3}Nb_{2/3}O_3$).

The manuscript is organized as follows. Section II contains a brief account of the technical details of the work, including the theoretical methods used, the slab geometries studied, and the formulation of the surface energy. In Sec. III we present the computed structural relaxations of the $PbTiO_3$ surfaces, and compare these to the previous results on $BaTiO_3$ and $SrTiO_3$ surfaces. Additionally, we discuss the surface energetics (surface energies and surface relaxation energies), and point out some characteristic differences in the surface electronic structure of the three compounds. Finally, the paper ends with a summary in Sec. IV.

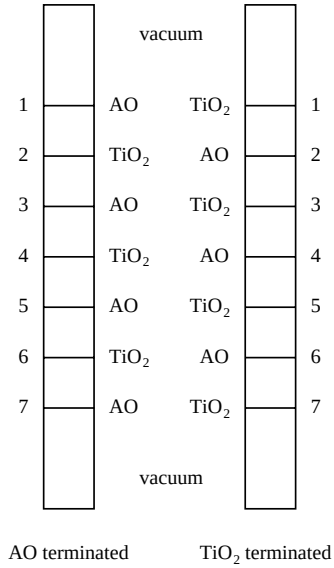

FIG. 1. Schematic illustration of the supercell geometries for the two differently terminated $ATiO_3$ (001) surfaces.

II. PRELIMINARIES

A. Theoretical Methods

We carried out self-consistent plane-wave pseudopotential calculations within Kohn-Sham density-functional theory using a conjugate-gradient technique.[15] Exchange and correlation were treated using the Ceperley-Alder form.[27] Vanderbilt ultrasoft pseudopotentials were employed,[28] with semicore Pb $5d$, Ba $5s$ and $5p$, Sr $4s$ and $4p$, and Ti $3s$ and $3p$ orbitals included as valence states. A plane-wave cutoff of 25 Ry has been used throughout. Relaxations of atomic coordinates are iterated until the forces are less than 0.01 eV/Å. Justification of the convergence and accuracy of this approach can be found in the previously published work.[9,11,15]

B. Surface and Slab Geometries

In this work we consider only II-IV cubic perovskites, i.e., ABO_3 perovskites in which atoms A and B are divalent and tetravalent, respectively. In this case, two non-polar (001) surface terminations are possible: the AO–terminated surface, and the BO_2–terminated surface.

We have studied both types of surface termination for all three materials ($PbTiO_3$, $BaTiO_3$, and $SrTiO_3$) using a repeated slab geometry. The slabs are symmetrically terminated and typically contain seven layers (17 or 18 atoms), as illustrated in Fig. 1. The vacuum region was chosen to be two lattice constants thick. The calculations were done using a (4,4,2) Monkhorst-Pack mesh,[29] corresponding to three or four k-points in the irreducible Brillouin zone for cubic and tetragonal surfaces respectively. The convergence of

the calculations has been very carefully checked for $PbTiO_3$ by repeating some of the calculations with asymmetrically terminated eight-layer slabs and symmetrically terminated nine-layer slabs. Additionally, we have enlarged the vacuum region to a thickness of three lattice constants, and we have checked the convergence of the Brillouin zone integration by going to a (6,6,2) k-point mesh. In all cases, the results for the structural properties of the surfaces given in the Tables I to V change by less than 0.2%.

For all three materials, we first computed the relaxations for the "cubic" surface, i.e., for the case where there is no symmetry lowering relative to a slab of ideal cubic material. In this case we preserved M_x, M_y, and M_z mirror symmetries relative to the center of the slab, and set the lattice constants in the $\hat{x}$ and $\hat{y}$ directions equal to those computed theoretically for the corresponding bulk material (3.89 Å, 3.95 Å, and 3.86 Å for $PbTiO_3$, $BaTiO_3$, and $SrTiO_3$, respectively). The symmetry-allowed displacements of the atoms in the z (surface-normal) direction were then fully relaxed.

Each of the three materials studied displays a different sequence of structural phase transitions from the cubic paraelectric phase as the temperature is lowered.[1] $PbTiO_3$ undergoes a single transition into a tetragonal ferroelectric (FE) phase at 763 K and then remains in this structure down to zero temperature. $BaTiO_3$ displays a series of three transitions to tetragonal, orthorhombic, and rhombohedral FE phases at 403 K, 278 K, and 183 K, respectively. $SrTiO_3$ remains cubic down to 105 K, at which point it undergoes an antiferrodistortive transition involving rotation of the oxygen octahedra and doubling of the unit cell. The material nearly goes ferroelectric at about $T = 30$ K, but is evidently prevented from doing so by quantum zero-point fluctuations.[30]

Because we are primarily interested in the room-temperature structures of these materials and their surfaces, we have chosen to focus on the tetragonal FE phases of $PbTiO_3$ and $BaTiO_3$ for our surface studies. We consider only the case of the tetragonal c axis (i.e., polarization) lying *parallel* to the surface, since polarization normal to the surface is strongly suppressed by the depolarization fields that would arise from the accumulated charge at the surfaces.[31] We take the tetragonal axis to lie along $\hat{x}$, and relax the M_x symmetry while retaining the M_y and M_z symmetries with respect to the center of the slab. For $PbTiO_3$, which is tetragonal at $T = 0$, this will indeed be the ground-state structure of the slab. For $BaTiO_3$, on the other hand, the M_y symmetry is artificially imposed so that the theoretical $T = 0$ calculation will mimic the experimental room-temperature surface structure. In both cases, the slab lattice constants in the $\hat{x}$ and $\hat{y}$ directions were set equal to the corresponding theoretical equilibrium lattice constants computed for the bulk tetragonal phase: c=4.04 Å and a=3.86 Å for $PbTiO_3$, and c=3.99 Å and a=3.94 Å for $BaTiO_3$.

C. Surface Energies

A comparison of the relative stability of the AO and TiO_2 surface terminations is problematic because the corresponding surface slabs contain different numbers of AO and TiO_2 formula subunits. We treat this problem by introducing chemical potentials μ_{AO} and μ_{TiO_2} for these subunits, defined in such a way that $\mu_{AO} = 0$ and $\mu_{TiO_2} = 0$ correspond to thermal equilibrium with bulk crystalline AO and TiO_2, respectively. We have computed the cohesive energies E_{AO} and E_{TiO_2} of crystalline PbO, BaO, SrO, and TiO_2 using the same

first-principles pseudopotential method in order to provide these reference values. The grand potential for a given surface structure can then be computed as

$$F_{\rm surf} = \frac{1}{2}[E_{\rm slab} - N_{\rm TiO_2}(E_{\rm TiO_2} + \mu_{\rm TiO_2}) - N_{\rm AO}(E_{\rm AO} + \mu_{\rm AO})] \ , \tag{1}$$

where N is the number of formula subunits contained in the slab, and the factor of $1/2$ accounts for the fact that each slab contains two surfaces. Assuming that the surface of the $ATiO_3$ is in equilibrium with its own bulk, it follows that

$$\mu_{\rm AO} + \mu_{\rm TiO_2} = -E_{\rm f} \ , \tag{2}$$

where $E_{\rm f}$ is the heat of formation of bulk $ATiO_3$ from bulk AO and bulk TiO_2. The two chemical potentials are thus not independent, and we choose to treat $\mu_{\rm TiO_2}$ as the independent variable when presenting our results. Accordingly, $\mu_{\rm TiO_2}$ is allowed to vary over the range

$$-E_{\rm f} \leq \mu_{\rm TiO_2} \leq 0 \ , \tag{3}$$

the lower and upper limit corresponding to the precipitation of particulates of AO and TiO_2 on the surface, respectively.

III. RESULTS AND DISCUSSIONS

A. Structural relaxations

We begin by presenting our new results on the structural properties of the $PbTiO_3$ (001) surfaces. The equilibrium atomic positions for both surface terminations in the two phases were obtained by starting from the ideal structures of the surfaces and then relaxing the atomic positions while preserving the symmetries described in section II B. The results for the fully relaxed geometries are summarized in Table I and II. By symmetry, there are no forces along $\widehat{x}$ and $\widehat{y}$ for the cubic surface, and no forces along $\widehat{y}$ for the tetragonal surface.

Tables I and II show for both surfaces a substantial inward contraction towards the bulk for the uppermost surface layers, whereas for the second layers we find an outward relaxation of the atoms relative to the positions of the atoms on the ideal surface. Generally, the metal and the oxygen atoms move in the same direction, but the relaxations of the metal atoms are much larger, leading to a rumpling of the layers. The single exception is the surface layer of the tetragonal TiO_2–terminated surface, where one of the two oxygen atoms moves in the opposite direction to the metal atom. Therefore we can see here a significant asymmetry between the O atoms with respect to their positions perpendicular to the surface. This asymmetry between the oxygen atoms in the topmost surface layer of the tetragonal TiO_2–terminated surface was also found for $BaTiO_3$ but with a much smaller amplitude. As expected, we find the largest relaxations for the surface–layer atoms, but the displacement of the Pb atom in the second layer of the TiO_2–terminated surface is of the same magnitude.

In order to compare these results with previous calculations for $SrTiO_3$ and $BaTiO_3$, we have calculated the changes in the interlayer distances Δd_{ij} and the amplitudes of the rumpling η_i of the layers in the surface slabs for all three perovskites. The results for both

Atom	$\delta_z(C)$	$\delta_x(T)$	$\delta_z(T)$
Pb(1)	−4.36	−3.44	−2.38
$O_{III}(1)$	−0.46	+11.85	−1.17
Ti(2)	+2.39	+3.62	+1.15
$O_I(2)$	+1.21	+9.27	+0.81
$O_{II}(2)$	+1.21	+11.45	+0.06
Pb(3)	−1.37	+0.00	−0.81
$O_{III}(3)$	−0.20	+11.14	−0.17
Ti(4)	0	+3.86	0
$O_I(4)$	0	+9.60	0
$O_{II}(4)$	0	+10.98	0

TABLE I. Atomic relaxations (relative to ideal atomic positions) of the PbO–terminated surface in the cubic (C) and tetragonal (T) phases. The relaxations perpendicular (δ_z) and parallel (δ_x) to the surface are given in percent of the lattice constants a and c, respectively. For reference, the theoretical δ_x values in the bulk ferroelectric phase, relative to the Pb atoms, are $\delta_x(\mathrm{Ti}) = 3.45$, $\delta_x(\mathrm{O_I}) = 9.26$ and $\delta_x(\mathrm{O_{II}}) = \delta_x(\mathrm{O_{III}}) = 10.44$. Atom labels refer to Figs. 2 and 1; results are only given for the top half of the slab, since the bottom half is equivalent by M_z mirror symmetry.

Atom	$\delta_z(C)$	$\delta_x(T)$	$\delta_z(T)$
Ti(1)	−3.40	+3.62	−3.47
$O_I(1)$	−0.34	+9.27	−1.60
$O_{II}(1)$	−0.34	+11.45	+0.79
Pb(2)	+4.53	+0.00	+4.06
$O_{III}(2)$	+0.43	+11.14	+0.17
Ti(3)	−0.92	+3.86	−0.79
$O_I(3)$	−0.27	+9.60	−0.03
$O_{II}(3)$	−0.27	+10.98	−0.06
Pb(4)	0	−3.44	0
$O_{III}(4)$	0	+11.85	0

TABLE II. Atomic relaxations of the TiO_2–terminated surface in the cubic (C) and tetragonal (T) phases. Notation is the same as in Table I.

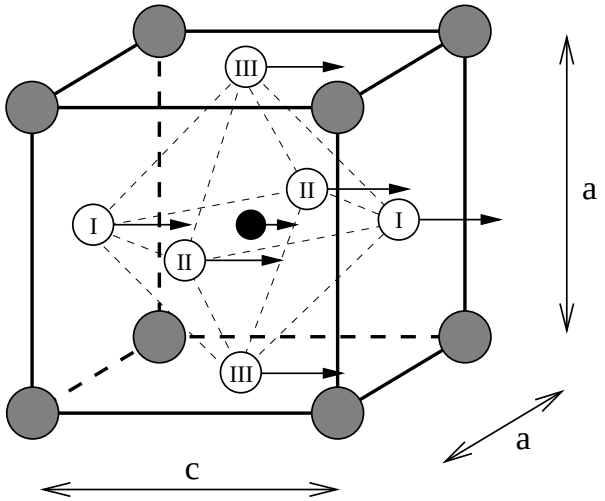

FIG. 2. Structure of the cubic perovskite compounds $ATiO_3$. Atoms A, Ti and O are represented by shaded, solid and open circles, and O_I, O_{II} and O_{III} are the oxygen atoms lying along the $\widehat{x}$, $\widehat{y}$ and $\widehat{z}$ direction from the Ti atom, respectively. Arrows indicate the displacements of the Ti and O atoms relative to the A atoms in the case of the tetragonal phase of $PbTiO_3$.

surface terminations and the different phases are given in the Tables III and IV. We denote the change in the z position of a metal atom relative to the ideal unrelaxed structure as $\delta_z(\mathrm{M})$, and $\delta_z(\mathrm{O})$ is the same for the oxygen atom in the same layer (defined as $[\delta_z(\mathrm{O_I}) + \delta_z(\mathrm{O_{II}})]/2$ for a TiO_2 layer). We then define the change of the interlayer distance Δd_{ij} as the difference between the averaged atomic displacements $[\delta_z(\mathrm{M}) + \delta_z(\mathrm{O})]/2$ of layer i and j, and the rumpling η_i is defined as the amplitude of these displacements $|\delta_z(\mathrm{M}) - \delta_z(\mathrm{O})|$. From Tables III and IV we can see that, for all three perovskites and for both terminations, the surfaces display a similar oscillating relaxation pattern with a reduction of the interlayer distance d_{12}, an expansion of d_{23} and again a reduction for d_{34}. However, compared to $BaTiO_3$ and $SrTiO_3$, the amplitudes of the relaxations in $PbTiO_3$ are significantly increased.

The second interesting feature of Tables III and IV is that for $BaTiO_3$, there is almost no difference in the relaxations of the surface layers between the cubic and the tetragonal phase. The same is true for the TiO_2–terminated surface of $PbTiO_3$. For the PbO–terminated surface, in contrast, the changes in the interlayer distances and the layer rumplings are strongly reduced in the tetragonal phase. We will come back to this point at the end of the next subsection.

B. Influence of the surface upon ferroelectricity

We turn now to the question of whether the presence of the surface has a strong effect upon the near–surface ferroelectricity. To analyze whether the ferroelectric order is enhanced or suppressed near the surface, we introduce average ferroelectric distortions δ_{FE} for each layer of the surface slabs:

$$\begin{aligned} \delta_{\mathrm{FE}} &= |\delta_x(\mathrm{A}) - \delta_x(\mathrm{O_{III}})| && \text{for AO planes and} \\ \delta_{\mathrm{FE}} &= |\delta_x(\mathrm{Ti}) - [\delta_x(\mathrm{O_I}) + \delta_x(\mathrm{O_{II}})]/2| && \text{for } TiO_2 \text{ planes.} \end{aligned} \tag{4}$$

	$SrTiO_3$	$BaTiO_3$		$PbTiO_3$	
	cubic	cubic	tetrag	cubic	tetrag
Δd_{12}	−3.4	−2.8	−2.8	−4.2	−2.6
Δd_{23}	+1.2	+1.1	+1.1	+2.6	+1.3
Δd_{34}	−0.6	−0.4	−0.4	−0.8	−0.5
η_1	5.8	1.4	1.5	3.9	1.2
η_2	1.2	0.4	0.5	1.2	0.7
η_3	1.1	0.3	0.4	1.2	0.6

TABLE III. Change of the interlayer distance Δd_{ij} and layer rumpling η_i (in percent of the lattice constant a) for the relaxed AO–terminated surface of the three perovskites in the cubic and tetragonal phases.

	$SrTiO_3$	$BaTiO_3$		$PbTiO_3$	
	cubic	cubic	tetrag	cubic	tetrag
Δd_{12}	−3.5	−3.1	−2.9	−4.4	−4.1
Δd_{23}	+1.6	+0.9	+1.2	+3.1	+2.5
Δd_{34}	−0.6	−0.6	−0.4	−0.6	−0.4
η_1	1.8	2.3	2.5	3.1	3.1
η_2	3.0	1.9	2.1	4.1	3.9
η_3	0.2	0.4	0.4	0.7	0.8

TABLE IV. Change of the interlayer distance Δd_{ij} and layer rumpling η_i (in percent of the lattice constant a) for the relaxed TiO_2–terminated surface of the three perovskites in the cubic and tetragonal phases.

	AO–terminated				TiO_2–terminated			
	$BaTiO_3$		$PbTiO_3$		$BaTiO_3$		$PbTiO_3$	
layer	δ_{FE}(BaO)	δ_{FE}(TiO_2)	δ_{FE}(PbO)	δ_{FE}(TiO_2)	δ_{FE}(BaO)	δ_{FE}(TiO_2)	δ_{FE}(PbO)	δ_{FE}(TiO_2)
1	1.6		15.3			4.4		5.7
2		1.8		6.8	1.4		7.0	
3	1.3		11.1			3.4		6.3
4		2.6		6.4	1.7		9.7	
bulk	1.5	3.2	10.4	6.4	1.5	3.2	10.4	6.4

TABLE V. Average layer-by-layer ferroelectric distortions δ_{FE} of the relaxed slabs, in percent of the lattice constant c. Last row shows the theoretical bulk values for reference.

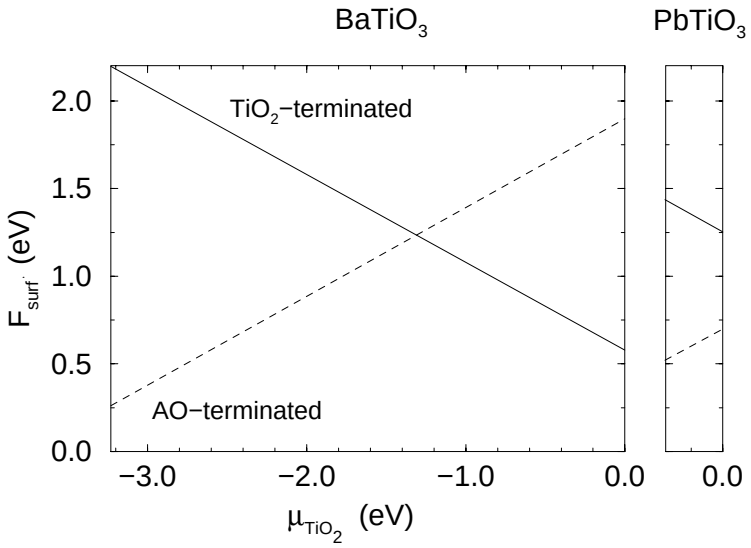

FIG. 3. Grand thermodynamic potential $F_{\rm surf}$ as a function of the chemical potential $\mu_{\rm TiO_2}$ for the two types of surfaces of $BaTiO_3$ (left) and $PbTiO_3$ (right), in the tetragonal phase. Dashed and solid lines correspond to AO–terminated and TiO_2–terminated surfaces, respectively.

The calculated values of $\delta_{\rm FE}$ for $BaTiO_3$ and $PbTiO_3$ are given in Table V; the last row of the table gives the bulk values for reference.

For the PbO–terminated surface of $PbTiO_3$, one can see a clear increase in the average ferroelectric distortions $\delta_{\rm FE}$ when going from the bulk values to the surface layer. On the other hand, for the TiO_2–terminated surface, the average distortions are slightly decreased at the surface. Surprisingly, this is just the opposite of what one observes for $BaTiO_3$, where one sees a reduction of the ferroelectric distortions for the BaO–terminated surface and a moderate enhancement for the TiO_2–terminated surface. (Of course, the distortions are also much smaller for $BaTiO_3$ surfaces, as they are in the bulk, compared to $PbTiO_3$.) These results tend to confirm that Pb is a much more active constituent in $PbTiO_3$ than is Ba in $BaTiO_3$, presumably because of the partially covalent nature of the Pb–O bonds as discussed in Sec. I.

In any case, the present results again confirm that the presence of the surface does not lead to any drastic suppression of the ferroelectric order near the surface, supporting the view that extrinsic effects must be responsible for degradation of ferroelectricity in thin-film geometries.

Finally, we note that there are interesting signs of interplay between the relaxations parallel and perpendicular to the surface for $PbTiO_3$. In particular, the relaxations perpendicular to the surface are substantially reduced (by a factor of $\sim$3) on the PbO-terminated surface when going from the cubic to the tetragonal case. This can be rationalized as follows. Because of the partial covalency of the Pb–O bonds, there is a tendency to reduce the Pb–O bond length (this length is 2.75, 2.51, and 2.30 Å in cubic $PbTiO_3$, tetragonal $PbTiO_3$, and PbO, respectively). For the cubic surface, by symmetry, the only possibility to shorten this bond length is by a strong movement of the Pb atom towards the bulk and a strong movement upwards of the O atoms in the second layer. This leads to the strong rumpling and the decrease of d_{12}. But in the tetragonal phase there is also the possibility

	$SrTiO_3$	$BaTiO_3$		$PbTiO_3$	
	cubic	cubic	tetrag	cubic	tetrag
E_f	3.2	3.20	3.23	0.30	0.36
E_{surf}	1.26	1.24	1.24	0.97	0.97
E_{relax}	0.18	0.13		0.21	0.22

TABLE VI. Formation energy E_f, average surface energy E_{surf} and average relaxation energy E_{relax} (in eV/unit cell) for the three perovskites in the cubic and tetragonal phases.

to enlarge the ferroelectric distortion in order to shorten the Pb–O bond length. Evidently, the enlargement of the ferroelectric distortion is preferred to the relaxation perpendicular to the surface.

C. Surface energies

In this section we discuss the surface energetics of the three perovskite compounds. In order to compare the relative stability of the AO– and TiO_2–terminated surfaces, we have calculated the grand thermodynamic potential F_{surf} (as introduced in Sec. II C) for the different surfaces as a function of the chemical potential μ_{TiO_2}. The results for the tetragonal surfaces of $BaTiO_3$ and $PbTiO_3$ are shown in Fig. 3. The graphs of the grand thermodynamic potentials for the $SrTiO_3$ surfaces are very similar to those of $BaTiO_3$ and are therefore not shown separately.

Figure 3 shows a very different behavior for the $BaTiO_3$ and $PbTiO_3$ surfaces. First of all, the formation energy E_f of $PbTiO_3$ (when formed from bulk PbO and TiO_2) is 0.36 eV, much lower than the formation energies of $SrTiO_3$ and $BaTiO_3$ which are about 3.2 eV. This leads to a much smaller range for the chemical potential μ_{TiO_2} for which $PbTiO_3$ surfaces can grow in thermodynamic equilibrium. Second, for $BaTiO_3$ the two different surfaces have a comparable range of thermodynamic stability, indicating that either BaO–terminated surfaces or TiO_2–terminated surfaces could be formed depending on whether growth occurs in Ba–rich or Ti–rich conditions. In contrast, for $PbTiO_3$ only the PbO–terminated surface can be obtained in thermodynamic equilibrium.

To get a quantity describing the surface energetics that is independent of the chemical potential μ_{TiO_2} and therefore allows a more direct comparison of the three compounds, we define the average surface energy per surface unit cell

$$E_{surf} = \frac{1}{4}\Big(E_{slab}^{AO} + E_{slab}^{TiO_2} - 7\,E_{bulk}\Big)\,, \tag{5}$$

which is equal to the average of the grand thermodynamic potential F_{surf} for the two kinds of surfaces. Again, the results for E_{surf} shown in Table VI are very similar for $SrTiO_3$ and $BaTiO_3$, whereas the value for $PbTiO_3$ is significantly lower.

Finally we have computed the average relaxation energy E_{relax} of the three perovskite compounds. E_{relax} is defined as the difference between the average surface energy E_{surf} of the ideal surface without relaxation of the atoms, and the fully relaxed surfaces. The largest

	$SrTiO_3$	$BaTiO_3$		$PbTiO_3$	
	cubic	cubic	tetrag	cubic	tetrag
AO-term.	1.86	1.80	2.01	1.53	2.12
TiO_2-term.	1.13	0.84	1.18	1.61	1.79
bulk	1.85	1.79	1.80	1.54	1.56

TABLE VII. Calculated band gaps (in eV) for the relaxed cubic and tetragonal surface slabs.

and smallest value for $E_{\rm relax}$ (see Table VI) were found for $PbTiO_3$ and $BaTiO_3$, respectively, which is in agreement with the observation that the atomic relaxations are largest in $PbTiO_3$ and smallest in $BaTiO_3$.

For all three compounds the average relaxation energy $E_{\rm relax}$ is many times larger than a typical bulk ferroelectric well depth, which is approximately 0.03 eV for $BaTiO_3$ and 0.05 eV for $PbTiO_3$. This would indicate that the surface is capable of acting as a strong perturbation on the ferroelectric order. As we have shown in Sec. III B, this is not the case for $BaTiO_3$ and $PbTiO_3$. One reason why the ferroelectric order is not as strongly affected by the surface as one might have thought has been pointed out in Ref. 9: the soft phonon eigenmode, which is responsible for the ferroelectric distortion, is only one of three zone center modes having the same symmetry. By looking at how strongly the surface relaxations are related to each of these zone center modes it has turned out that the distortions induced by the presence of the surface are to a large extent of non–ferroelectric character.

D. Surface band structure

For all three perovskite compounds we have carried out LDA calculations of the bulk and the surface electronic structure for our various surface slabs. It is well known that the LDA is quantitatively unreliable regarding excitation properties such as band gaps. Since we are in the following only looking at differences between band structures, we think that our conclusions drawn from the LDA results are nevertheless qualitatively correct.

As has already been shown in Ref. 15, the bulk band structures of $SrTiO_3$ and $BaTiO_3$ are very similar, whereas $PbTiO_3$ shows some significant differences. In $SrTiO_3$ and $BaTiO_3$ the upper edge of the valence band is very flat throughout the Brillouin zone. On the other hand, in $PbTiO_3$ the shallow $6s$ semicore states of the Pb atoms hybridize with the $2p$ states of the O atoms, leading to a lifting of the upper valence band states near the X point of the Brillouin zone.

This fact is responsible for a different behavior of the $PbTiO_3$ surface band structure compared to $SrTiO_3$ and $BaTiO_3$. If we look at the calculated band gaps in Table VII, we see that for TiO_2–terminated surfaces the band gap is significantly reduced for $SrTiO_3$ and $BaTiO_3$, whereas for $PbTiO_3$ the band gap is almost unchanged. The reduction of the band gap in $SrTiO_3$ and $BaTiO_3$ is mainly due to an upward intrusion of the upper valence band states near the M point into the lower part of the band gap (as pointed out in Ref. 9, this is caused by the suppression of the hybridization of certain O $2p$ and Ti $3d$ orbitals in the

surface layer). In $PbTiO_3$ we find the same upward movement of the upper valence band states near the M point, but these states stay just below the highest valence states at the X point, and so the band gap is almost unchanged.

On the other hand, for the AO–terminated surfaces we see no reduction of the band gap for any of the three perovskite compounds. Even here, however, there is a subtle difference between $PbTiO_3$ and the other materials, this time concerning the conduction band edge. According to our calculations, the Pb $6p$ states overlap the Ti $3d$ states to some degree in bulk $PbTiO_3$, and this effect is accentuated at the Γ point of the surface Brillouin zone on the Pb–O terminated surface, where the lowest Pb $6p$ state falls just below the lowest Ti $3d$ state. We thus suggest that the conduction band minimum may actually have Pb $6p$ character at this surface, although the effect is too small to affect the band gaps in Table VII substantially. This might be an interesting target of investigation for future spectroscopic experimental studies.

IV. SUMMARY

In summary, we have calculated structural and electronic properties of $PbTiO_3$ (001) surfaces using a first-principles density-functional approach. The results are compared and contrasted with corresponding previous calculations on $BaTiO_3$ and $SrTiO_3$ surfaces. We observe qualitatively different behavior of the $PbTiO_3$ surfaces in several respects. First, within the narrow range of PbO and TiO_2 chemical potentials permitted by bulk thermodynamics, we find that the TiO_2-terminated surface is never thermodynamically stable. Thus, the PbO-terminated surface is expected to be the one observed experimentally. Second, the interaction between the ferroelectric distortion and the presence of the surface is quite different for $PbTiO_3$, compared to $BaTiO_3$. In particular, the ferroelectricity is strongly enhanced at the AO-terminated surface and suppressed at the TiO_2-terminated surface, just the opposite of the behavior found for $BaTiO_3$. Moreover, the ferroelectric distortion at the surface allows for a drastic reduction of the rumpling of the surface layer on the PbO-terminated surface, an effect which is not seen on the BaO-terminated of $BaTiO_3$. Third, the surface electronic band structure is qualitatively modified in the case of $PbTiO_3$ by the presence of Pb $6s$ and $6p$ states in the upper valence and lower conduction regions.

ACKNOWLEDGMENTS

This work was supported by the ONR grant N00014-97-1-0048.

REFERENCES

[1] M.E. Lines and A.M. Glass, *Principles and Applications of Ferroelectrics and Related Materials,* (Clarendon Press, Oxford, 1977); F. Jona and G. Shirane, *Ferroelectric Crystals,* (Dover Publications, New York, 1993).

[2] F. Tsai and J.M. Cowley, Appl. Phys. Lett. **65**, 1906 (1994).

[3] J.C. Niepce, *Surface and Interfaces of Ceramic Materials,* edited by L.C. Dufour (Kluver Academic Publishers, 1989), p. 521.

[4] V.E. Henrich and P.A. Cox, *The Surface Science of Metal Oxides,* (Cambridge University Press, New York, 1994).

[5] D. Vanderbilt, Current Opinions in Solid State and Materials Science **2**, 701 (1997).

[6] D. Vanderbilt, in *Proceedings of the Ninth International Meeting on Ferroelectrics,* Journal of the Korean Physical Society **32**, S103-S106 (1998).

[7] R.E. Cohen, J. Phys. Chem. Solids **57**, 1393 (1996).

[8] R.E. Cohen, Ferroelectrics **194**, 323 (1997).

[9] J. Padilla and D. Vanderbilt, Phys. Rev. B **56**, 1625 (1997).

[10] S. Kimura *et al.*, Phys. Rev. B **51**, 11049 (1995).

[11] J. Padilla and D. Vanderbilt, Surface Science **418**, 64 (1998).

[12] Z.-Q. Li, J.-L. Zhu, C.Q. Wu, Z. Tang, and Y. Kawazoe, Phys. Rev. B **58**, 8075 (1998).

[13] R.E. Cohen, Nature **358**, 136 (1992).

[14] R.E. Cohen and H. Krakauer, Ferroelectrics **136**, 65 (1992).

[15] R.D. King-Smith and D. Vanderbilt, Phys. Rev. B **49**, 5828 (1994).

[16] A. García and D. Vanderbilt, Phys. Rev. B **54**, 3817 (1996).

[17] U.V. Waghmare and K.M. Rabe, Ferroelectrics **194**, 135 (1997).

[18] W. Zhong and D. Vanderbilt, Phys. Rev. Lett. **74**, 2587 (1995).

[19] D.J. Singh, Phys. Rev. B **52**, 12559 (1995).

[20] L. Bellaiche, J. Padilla, and D. Vanderbilt, in *First-Principles Calculations for Ferroelectrics: Fifth Williamsburg Workshop*, R.E. Cohen, ed. (AIP, Woodbury, New York, 1998), p. 11.

[21] L. Bellaiche, J. Padilla and D. Vanderbilt, Phys. Rev. B **59**, 1834 (1999).

[22] T. Egami, W. Domowski, M. Akbas, and P.K. Davies, in *First-Principles Calculations for Ferroelectrics: Fifth Williamsburg Workshop*, R.E. Cohen, ed. (AIP, Woodbury, New York, 1998), p. 1.

[23] T. Hikita, T. Hanada and M. Kudo, Surface Science, **287/288**, 377 (1993).

[24] N. Bickel *et al.*, Vacuum **41**, 46 (1990); Phys. Rev. Lett. **62**, 2009 (1989).

[25] M. Naito, H. Sato, Physica C **229**, 1 (1994).

[26] K. Kitahama, Q. R. Feng, T. Kawai and S. Kawai, Bulletin of Fall Meeting of Japanese Applied Physics Society **2**, 494 (1992).

[27] D.M. Ceperley and B.J. Alder, Phys. Rev. Lett. **45**, 566 (1980).

[28] D. Vanderbilt, Phys. Rev. B **41**, 7892 (1990).

[29] H.J. Monkhorst and J.D. Pack, Phys. Rev. B **13**, 5188 (1976).

[30] W. Zhong and D. Vanderbilt, Phys. Rev. B **53**, 5047 (1996).

[31] W. Zhong, R. D. King-Smith and D. Vanderbilt, Phys. Rev. Lett. **72**, 3618 (1994).